Evaluation of materials defect influence on fatigue crack threshold

M. Leonavičius, K. Bobyliov, A. Krenevičius, S. Stupak*, E. Stupak

Vilnius Gediminas Technical University, Dept. of Strength of Materials, Saulėtekio ave 11, LT-10223 Vilnius, Lithuania

Received 16 May 2007, received in revised form 31 August 2007, accepted 31 August 2007

Abstract

The object of performed investigation is fatigue crack propagation in spheroid graphite cast iron with shrinkage voids. These voids influence on CT specimen's section properties has been evaluated. The decrease of the threshold ΔK_{th} obtained in specimens with voids compared to specimens without voids during natural tests has been investigated by means of different computational methods. The determined cracking threshold ΔK_{th} of investigated specimens without defects varies from 8.4 MPa $\sqrt{\mathrm{m}}$ up to 10 MPa $\sqrt{\mathrm{m}}$, of CT specimens with defects – from 6.3 MPa $\sqrt{\mathrm{m}}$ up to 8 MPa $\sqrt{\mathrm{m}}$. The comparison of stress intensity factor values obtained by analytical and numerical calculations shows a satisfactory similarity (with approx. 10 % difference).

K e y w o r d s: fracture, stress intensity factor, threshold, cast iron, defects

1. Introduction

Most spheroid graphite iron (SGI) properties are comparable to those of steel when yield and ultimate strength can be even higher than those of steel. The cast iron dumping property is 2–3 times higher than that of steel and together with a low sensitivity to stress concentration has a positive influence on strength properties in various loading modes, also the cyclic ones. SGI, as pig iron and steel properties combination, can be treated as a special engineering material used for transporting and mining parts production. Sometimes the service resistance to cyclic load is reduced by various casting defects that are often spread chaotically in a volume part. That is why a lifetime prediction method evaluating the influence of such defects is needed.

Shrinkage voids and porosity are basic casting defects [1–3]. They appear because during solidification the casting metal becomes denser. Shrinkage voids is a kind of porosity, so some conditions for its appearance should be fulfilled. Mostly it is not a thermal, but rather a pressure process. When the molten sprue becomes solid, the casting solidification process still continues and the pressure of still liquid metal is changing, at the same time a quantity of evolving gas appears. If casting part walls are thin, shrinkage voids can provoke the cavitation effects. The porosity evaluation in engineering calculation is difficult, so higher safety factors should be used [4–7]. Shrinkage voids and pores reduce mechanical properties of the part and also its section properties, meanwhile being on the casting surface, and they become crack sources.

Non-destructive defect control methods are widely used. Unfortunately, the porosity in casting dangerous sections is often too small to be found, but its influence can define service properties of the part. Quality standards preview only quantitative defects evaluation; meanwhile a subjective evaluation cannot assure service properties. It should be noticed that repeating shrinkage voids can be found and evaluated more easily than random gas porosity cases.

The analysis of casting and thermal treatment defects [1, 2, 8–10] shows that various structural anomalies have some specific attributes linked to technological process malfunctions and problems in controlling big cast iron parts casting, cooling and thermal treatment.

2. Structural analysis and mechanical properties

The chemical composition and microstructure of

*Corresponding author: tel.: +370 5 2744857; fax: +370 5 2744858; e-mail address: stupakas@adm.vtu.lt

Table 1. Chemical composition (wt.%)

C	Mn	Si	Mg	Cu	Mo	Ni
3.7	0.14 . . . 0.16	0.92 . . . 0.95	0.05 . . . 0.10	0.22 . . . 0.24	0.01 . . . 0.03	0.12 . . . 0.14

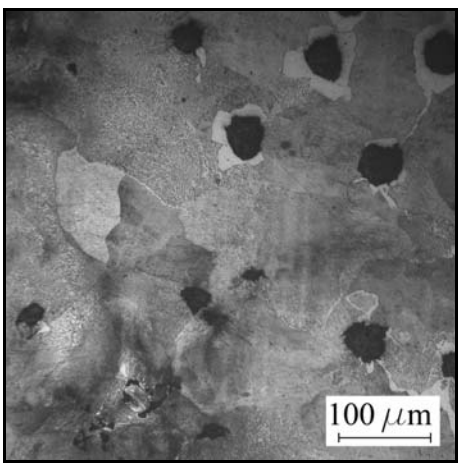

Fig. 1. Investigated cast iron micrograph. Shrinkage voids in left bottom corner. Graphite, pearlite matrix, white graphite envelopment – ferrite.

specimens shows that investigated specimens are made of SGI. The chemical composition is presented in Table 1.

Microstructure is shown in Fig. 1. This cast iron has a pearlite matrix, graphite inclusions are spherical. These inclusions are surrounded by a ferrite layer called "bull's eye". A little amount of ferrite is useful and ameliorates mechanical properties, because a fragile inclusion (graphite) is surrounded by a yielder layer, which absorbs (decelerates) micro- and macro--cracks. Neither graphite inclusions nor ferrite envelopment shape are regular enough. Graphite inclusions rate is about 150 globule cm^{-2}. Their size is 30 . . . 100 μm, and together with a low concentration it defines not quite high mechanical properties.

An interesting microstructure anomaly signs where it has a dendrite direction could be found in some specimen spots near to defects (Fig. 2). It happens due to an inversed silicon microliquation which results in dendrite axial area saturated with silicon. This structure anomaly significantly lowers cast iron mechanical properties.

Spherical-shape graphite inclusions define higher mechanical properties. Naturally, graphite gets a flake shape because of its structure. To obtain a spherical graphite shape, additional chemical elements should be added, for example, magnesium, which reacts with sulphur and oxygen. As a result, sulphur compound MgS and magnesium oxide MgO are got; consequently the surface stresses arise and the spherical shape is obtained. Adding 0.03 . . . 0.06 % Mg, negative sulphur effect is removed. In order to stimulate graphite inclusions appearance, some materials are added, mostly ferro-silicon. Graphite is being concentrated around silicon compound molecules, and also graphite intention to solidify in a metastable phase is eliminated.

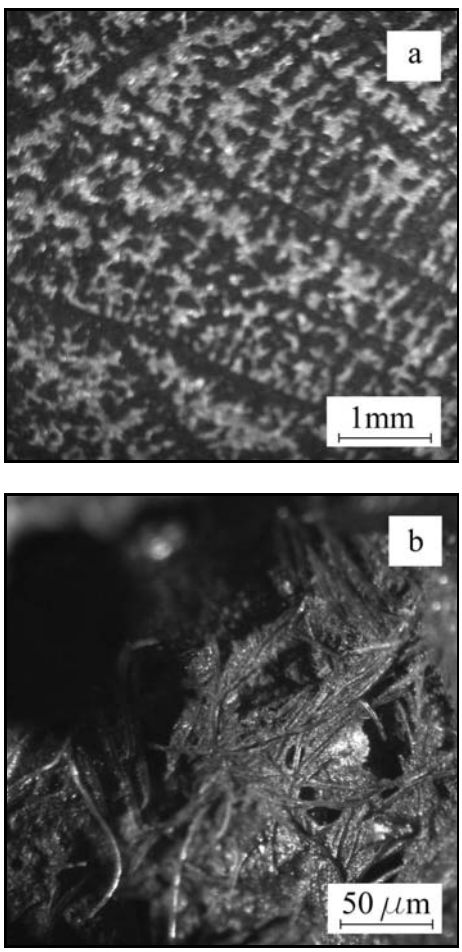

Fig. 2. Dendrites in cast iron: (a) dendrite orientation structure anomaly, (b) dendrites on compact specimen fracture surface.

Cylindrical tension specimens have been made to establish mechanical properties. These properties are: elasticity modulus $E = 175$ GPa; Poisson's ratio $\upsilon = 0.275$; yield strength $\sigma_{0.2} = 380 \ldots 405$ MPa; ultimate strength $\sigma_{\mathrm{u}} = 490 \ldots 515$ MPa; hardness – 210 . . . 240 BHN.

Experimental tests were made in compliance with the requirements established for work procedure (re-

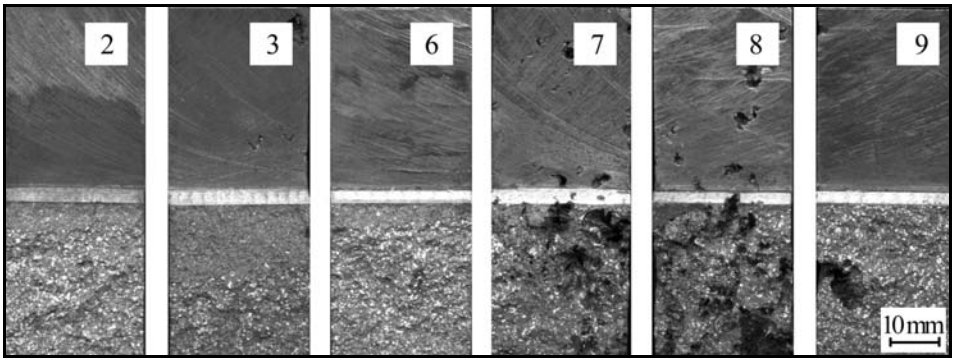

Fig. 3. Compact specimen fractures.

garding loading conditions, crack size and its measurements).

3. Experimental study

The resistance of cast iron to crack propagation under a cyclic loading was investigated experimentally by 9 compact specimens with main dimensions $W = 36$ mm and $B = 18$ mm. The stress intensity factor has been calculated according to standard ASTM E 647-00. An experimental research was performed when cycle asymmetry factor was 0.05 and crack propagation rate approaches 10^{-10} and 10^{-11} m/cycle. Specimens 1–6 had no defects, though defects of different sizes could be found on lateral faces. Specimens 7–9 contained defects on fracture surfaces, as well as on external faces. In samples without defects, the crack formation and propagation corresponded to the usual regularity. Fractures of CT specimen are shown in Fig. 3.

Voids distribution in the specimen 8 is shown in Fig. 4. Voids are inside and could be found by non-destructive control methods. However, their size and quantity are difficult to define both in the casting and in the structural element. Shrinkage and blowholes may also be found, both inside the casting and outside it. Their size, shape and distribution are different.

In specimens with defects the crack formation and propagation depend on many factors. In initial stage (when depth is 2–3 mm) the crack develops in the notch influence zone and is almost perpendicular to normal stresses, if there are no defects. For further propagation a great influence is exerted by the homogeneity of the material and the anisotropy of separate parts of structural elements. Defects and non-homogeneous anomalies around them change the strain state in the crack tip. The integral influence of metal structure in some zones predetermines the crack propagation, so that its trajectory passes crack planes and defects at different growing angles. In Figs. 3, 4 we see that the crack changes its direction not only at the specimen face but also inside. The crack reaches voids

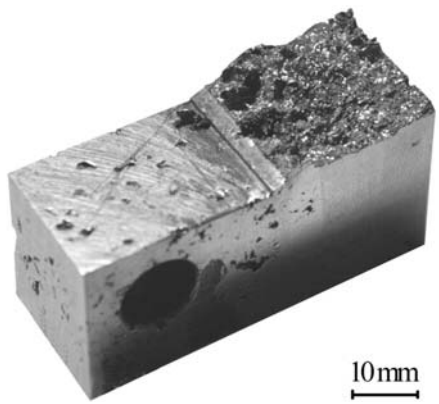

Fig. 4. Compact specimen with external and internal voids.

by a complicated trajectory in such a way that some macro-particles separate completely. A great influence is exerted by the structural properties nearby cracking threshold ΔK_{th}. Such sensitivity means that when propagating fatigue crack meets on its way structural zones with a different resistance, the stress state changes and conditions of normal break-off, transverse shear and longitudinal shear develop. Different load combinations can affect the specimen by thousands of cycles or for a short time and determine a complicated crack front trajectory, the zigzag crack development and also change its growth rate. It might be noticed that, in the initial stage, the defect changes the crack trajectory immediately, if it is close to notch tip (specimen 7, Fig. 4).

4. Analytical study

The calculation of geometrical indices of fracture with defects was reviewed in [11, 12]. Section properties of defective section with crack without assessment of defects and with assessment of defects are calculated in this way:

$$A = (W - a)B, \quad I = B(W - a)^3/12, \quad S = I/e_{\mathrm{c}},$$

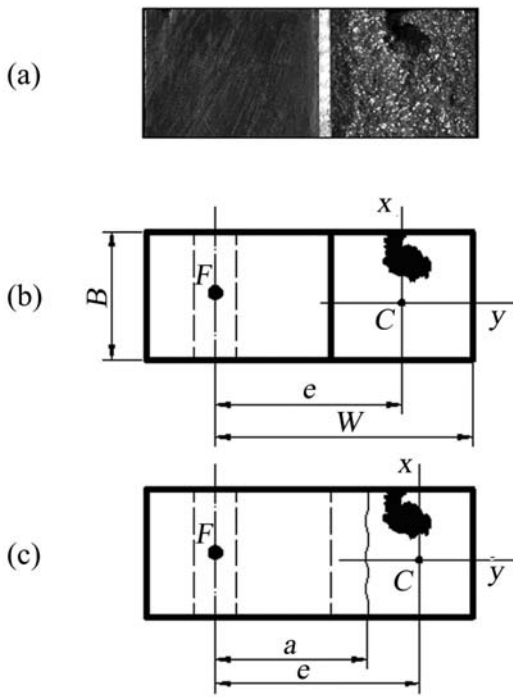

Fig. 5. Defective specimen: (a) fracture, (b) defective fracture scheme, (c) defective fracture scheme with crack (F – tension force apply point, C – net area centre, e – load eccentricity, a – crack depth).

$$A^* = \sum A_i^*, \quad I^* = \int_A x_i^2 \mathrm{d}A_i^*, \quad A_\mathrm{d} = A - A^*,$$

$$I_\mathrm{d} = I + A(e_\mathrm{c} - e_\mathrm{cd})^2 - (I^* + A^*(e^* - e_\mathrm{cd})^2),$$

$$S_\mathrm{d} = I/e_\mathrm{cd}, \quad e_\mathrm{c} = (W - a)/2, \quad e^* = \sum A_i^* x_i / A^*,$$

$$e_\mathrm{cd} = e_\mathrm{c} + A^*(e^* - e_\mathrm{c})/A_\mathrm{d}, \quad i = 1, 2, ..., n, \tag{1}$$

where A, I, S are section area, moment of inertia, and section modulus of fracture with defects (n is number of defects) without assessment of defects; A_d, I_d, S_d are correspondingly section area, moment of inertia, and section modulus of fracture with defects with assessment of defects; A^*, e^* and I^* are area and its centroid distance from crack front and moment of inertia about centroid axis z of CT fracture defects obtained in AutoCAD; e_c and e_cd are CT fracture surface centroid distance from crack front without assessment of defects and with assessment of defects correspondingly (see Fig. 5). The stress intensity factor has been calculated according to the standard ASTM E 647-00:

$$K = \frac{F}{B \cdot W^{1/2}} f(\lambda),$$

$$f(\lambda) = \left[(2+\lambda)/(1-\lambda)^{3/2}\right] \varphi(\lambda), \quad \lambda = a/W, \tag{2}$$

$$\varphi(\lambda) = \left(0.866 + 4.64\lambda - 13.32\lambda^2 + 14.72\lambda^3 - 5.6\lambda^4\right),$$

where F is tension force, a is crack depth.

The expression (2) may also be written in this way:

$$\begin{aligned} K &= (F/BW^{1/2})[(2+\lambda)/(1-\lambda)^{3/2}]\varphi(\lambda) = \\ &= (F/BW^{1/2})[(2+\lambda)(1-\lambda)^{1/2}/(1-\lambda)^2]\varphi(\lambda) = \\ &= (F/BW^{1/2})2W \times [(2+\lambda)(1-\lambda)^{1/2}/ \\ &\quad ((1-\lambda)^2 2W)]\varphi(\lambda). \end{aligned} \tag{3}$$

Further efforts were made to determine what influence on propagating crack growth had the weakening of the defective specimen due to lower cross-section and other geometrical indices.

The nominal normal stress at the crack tip is calculated in the following way:

$$\sigma = \left(\frac{2F}{BW}\right) \frac{(2+\lambda)}{(1-\lambda)^2}. \tag{4}$$

By inserting this expression in Eq. (2) the following formula for calculating the stress intensity factor is obtained:

$$K_\mathrm{d} = 0.5\sigma\, W^{1/2}(1-\lambda)^{1/2}\varphi(\lambda). \tag{5}$$

The real nominal stresses differ from the calculated ones according to Eq. (3), because the geometric indices are lower due to defects in the fracture. With regard to changing geometric indices, the real nominal stresses are calculated in this way:

$$\sigma_\mathrm{d} = F/A + M/S, \tag{6}$$

where A is real area of the cross-section, S is real section modulus. By putting the results of expression (5) into (4), it is possible to calculate the real stress intensity factor:

$$K = 0.5\sigma_\mathrm{d} W^{1/2}(1-\lambda)^{1/2}\varphi(\lambda). \tag{7}$$

Therefore the obtained stress intensity factor threshold ΔK_th of specimens with defects is conventional because a presumption is made that the crack is perpendicular to normal stresses. But it should be mentioned that the results obtained with three CT specimens with defects are similar. The fatigue crack growth rate (calculated according to obtained results) is presented separately for specimens without defects in Fig. 6a and for specimens with defects in Fig. 6b.

By post-processing the stress intensity factor according to Eq. (7), new defective specimens' kinetic diagrams have been obtained. Figure 6 shows that after post-processing defective specimens crack growth rates are close to the ones without defects.

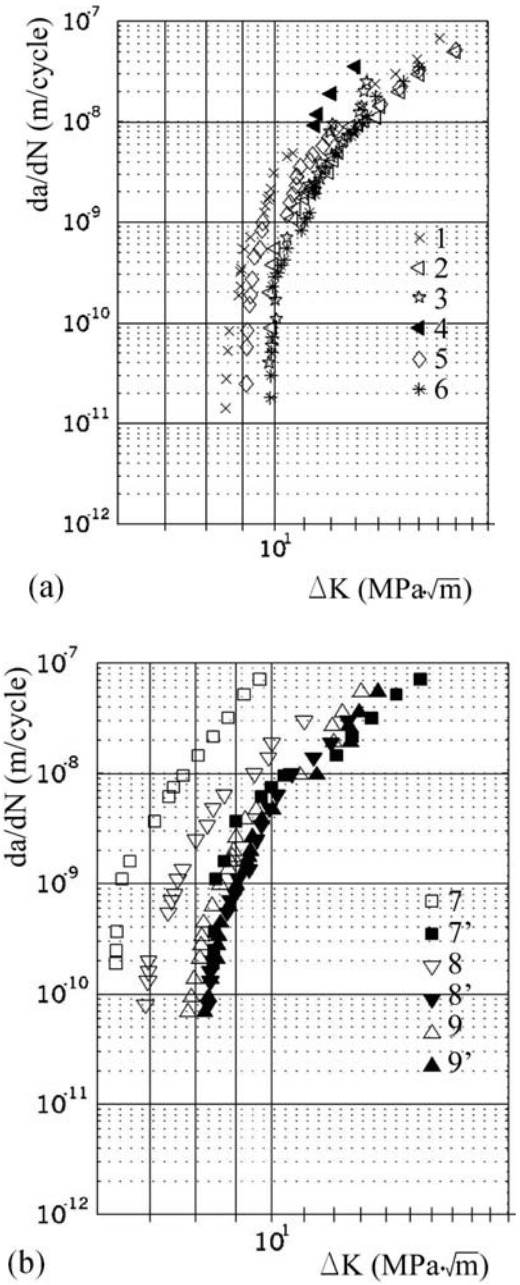

Fig. 6. Fatigue crack growth: (a) CT without defects, (b) CT with defects: ■,▼, ▲ – data calculated according to (4) for specimens 7, 8, 9; □, ▽, △ – data calculated according to (6) for specimens 7, 8, 9.

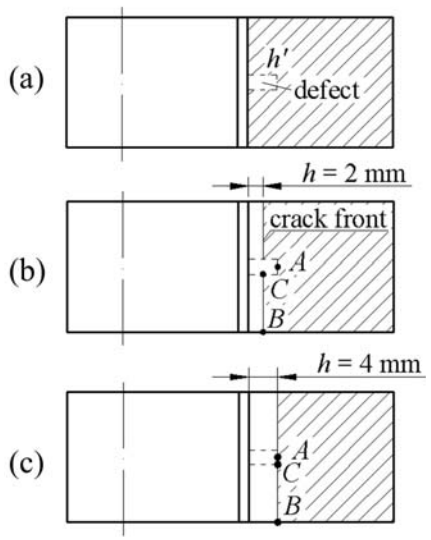

Fig. 7. Plane of the defective section with crack: h – depth of crack, h' – size of defect; (a) scheme of defective section with crack, (b) crack with 2 mm depth, (c) crack with 4 mm depth.

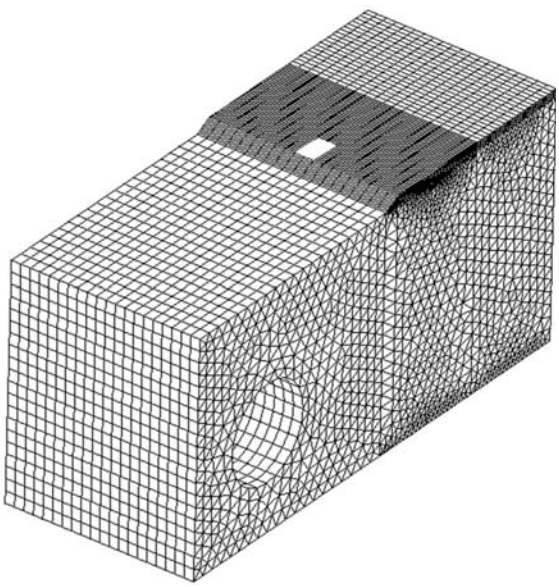

Fig. 8. FE mesh of CT specimen model with artificial defect.

Figure 6 also shows that specimens with defects are much less resistant to crack propagation than those without defects. The latter specimens crack growth experimental data are presented in the left field comparing to specimens with defects. The crack threshold for specimens without defects $\Delta K_{\rm th} = 8.4 \ldots 10$ MPa $\sqrt{\rm m}$. The crack threshold for specimens with defects $\Delta K_{\rm thd} = 6.3 \ldots 8$ MPa $\sqrt{\rm m}$. Reviewing the edges of defects in specimens 7, 8 and 9 after testing, it has been found that voids were not a crack development source.

Numerical aspects of voided material fracture strength are analysed in [13, 14]. ANSYS simulation for a defective model was performed to evaluate the defect influence on stress intensity factor. The defect has been initiated at the notch of specimen and has a rectangle shape as presented in Fig. 7.

Defect height (h' in Fig. 7a) was 4 mm, width was 2 mm. Relative crack depth varies from 0.4 to 4 mm. In Fig. 7b,c two different positions of crack are presented:

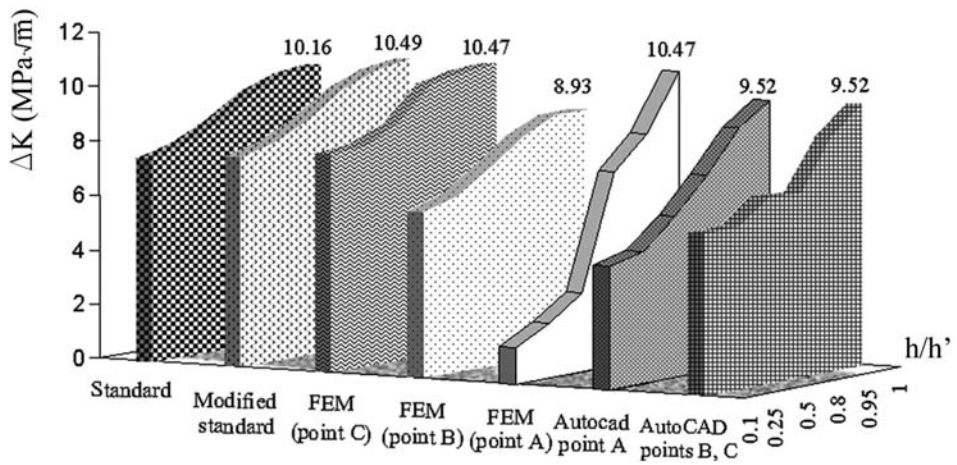

Fig. 9. Stress intensity factor (SIF) versus normalized crack depth (h/h').

with 2 mm and 4 mm depth. Stress intensity factor values were calculated in points A, B, C which are presented in Fig. 7b,c: point A is selected in front edge of defect, B – on crack intersection with free surface of CT point, C – on crack intersection with lateral edge of defect point. Crack front was straight in calculation by standard formulas and has the shape of multiline (excluding $h = h'$) in ANSYS simulation. FE mesh has been generated using triangle and rectangular elements in plane. After they were modified to 3D brick elements, using layers technique. FE mesh used for stress intensity factor calculation is presented in Fig. 8.

Calculated factor values are presented in Fig. 9. Natural tests results are given for comparison purposes only. Values obtained by FEM, using J-integral calculated by different integrations paths, show that defect has an influence on the stress intensity factor. The most considerable influence is found in front edge of defect, point A (Fig. 7). For comparison, a similar calculation by AutoCAD is also shown. Though values obtained by AutoCAD simulation are comparable to FEM simulation results, it is necessary to notice that they are not sensitive to strain state triaxility and stress concentration (that's why values in points B and C are equal).

The performed experimental analytical investigation may be applied in engineering calculations. If a void in a casting is found, its dimensions, area and volume should be defined. It is possible to use minimal ΔK_{thd} value in calculating of limit stresses $\Delta\sigma_{\mathrm{thd}}$ of a real structural element.

5. Conclusions

1. Microstructure anomalies and graphite structure have an influence on static mechanical properties of cast iron and on its resistance to cyclic loads.

2. Fracture analysis shows that defects deform crack front. Dendrites found around defects are less resistant than basic metal matrix, and it influences the crack propagation.

3. The defined cracking threshold ΔK_{th} of investigated specimens without defects varies from 8.4 MPa $\sqrt{\mathrm{m}}$ up to 10 MPa $\sqrt{\mathrm{m}}$, of CT specimens with defects – from 6.3 MPa $\sqrt{\mathrm{m}}$ up to 8 MPa $\sqrt{\mathrm{m}}$.

4. The comparison of stress intensity factor values obtained by analytical and numerical calculations shows a satisfactory similarity (with approx. 10 % difference).

References

[1] BUDINSKI, K. G.—BUDINSKI, M. K.: Engineering Materials: Properties and Selection. Pearson, Prentice Hall 2005.
[2] GOODRICH, G. M.: Cast Iron Microstructure Anomalies and Their Cause. AFS Transactions. Illinois, Inc., Des Plaines, American Foundry Society 1997, p. 669.
[3] LEONAVIČIUS, M.—PETRAITIS, G.—KRENEVIČIUS, A.—ŠUKŠTA, M.— STUPAK, S.: Kovove Mater., *43*, 2005, p. 348.
[4] BROEK, D.: The Practical Uses Fracture Mechanics. Dordrecht/Boston/London, Kluwer Academic Publishers 1989.
[5] STOYCHEV, S.—KUJAWSKI, D.: I. J. Fatigue, *27*, 2005, p. 1425.
[6] LI-CHUN BIAN, J.: I. J. Fatigue, *25*, 2003, p. 521.
[7] NEWMAN, J. C. Jr.—PHILIPS, E. P.—SWAIN, N. H.: I. J. Fatigue, *21*, 1999, p. 109.
[8] TROSHCHENKO, V.: Deformation and Fracture of Metals in High Cyclic Loading. Kijev, Naukova Dumka 1981 (in Russian).
[9] ŽVINYS, J.: Structural Alloys. Cast Iron. Kaunas, Technologija 1999.
[10] TROSHCHENKO, V. T.: Mechanika, *49*, 2004, p. 5.

[11] STUPAK, S.—LEONAVIČIUS, M.—BOBYLIOV, K.: In: Proceedings of 11th Int. Conference MECHANIKA 2006. Eds.: Daunys, M., Bazaras, Ž. Kaunas, Lithuana, Kaunas University of Technology 2006, p. 335.
[12] ASTM E 647–00. Standard Test Method for Measurement of Fatigue Crack Growth Rates, 2000.
[13] KAČIANAUSKAS, R.—STUPAK, E.—STUPAK, S.: Mechanika, *51*, 2005, p. 18.
[14] NADOT, Y. —BILLAUDEAU, T.: Engineering Fracture Mechanics, *73*, 2006, p. 112.